Journal of Power Sources 185 (2008) 615–620

Contents lists available at ScienceDirect

Journal of Power Sources

journal homepage: www.elsevier.com/locate/jpowsour

Supported PtRu on mesoporous carbons for direct methanol fuel cells

Catia Arbizzani, Sabina Beninati, Francesca Soavi, Alberto Varzi, Marina Mastragostino*

University of Bologna, Department of Metal Science, Electrochemistry and Chemical Techniques, via San Donato 15, 40127 Bologna, Italy

ARTICLE INFO

Article history:
Received 24 July 2008
Received in revised form 2 September 2008
Accepted 10 September 2008
Available online 18 September 2008

Keywords:
Direct methanol fuel cell
DMFC
Mesoporous carbon
PtRu
Supported electrocatalyst

ABSTRACT

We prepared and characterized several cryogel mesoporous carbons of different pore size distribution and report the catalytic activity of PtRu supported on mesoporous carbons of pore size >15 nm in passive and in active direct methanol fuel cells (DMFCs). At room temperature (RT), the specific maximum power of the passive DMFCs with mesoporous carbon/PtRu systems as anode was in the range 3–5 W g^{-1}. Passive DMFC assembly and RT tests limit the performance of the electrocatalytic systems and the anodes were thus tested in active DMFCs at 30, 60 and 80 °C. Their responses were also compared to those of commercial Vulcan carbon/PtRu. At 80 °C, the specific maximum power of the active DMFC with C656/PtRu was 37 W g^{-1} and the required amount of Pt per kW estimated at 0.4 V cell voltage was 31 g kW^{-1}, a value less than half that of Vulcan carbon/PtRu.

1. Introduction

Since 1992, when the first direct methanol fuel cells (DMFCs) operating with a Nafion membrane were developed with a design close to that of today, this type of fuel cell has been extensively studied for medium-low temperature applications. At present, DMFCs are mainly envisaged for portable power sources, which require high energy density, compact design and easy refuelling. This is particularly true of passive DMFCs, which operate under air breathing and methanol diffusion from a reservoir and are favoured by developers of mobile phones [1,2].

However, the high loading of noble metal catalyst of the electrodes still remains the major problem for these fuel cells. While the performance of H_2 fed proton exchange membrane fuel cells (PEMFCs) is limited by the slow kinetics of oxygen reduction at the cathode, that of DMFCs is also affected by the slow methanol oxidation at the anode and, hence, the catalyst loading required in DMFCs is higher than that in PEMFCs [3]. A high loading of noble metal, even higher if DMFCs operate in passive mode, negatively affects the cost of DMFCs, already hampered by the cost of the Nafion membrane. It is well known that the best performing catalyst for methanol oxidation is unsupported or carbon supported PtRu. Although carbon supported PtRu provides maximum utilization of the catalyst particles and prevents metal agglomeration [4–10], the unsupported is used for cell assembly of high catalyst loading (up to 10 mg_{Pt} cm^{-2}) [10].

Together with the poor kinetics of methanol oxidation, another issue is methanol crossover through the polymer membrane which at the cathode generates a mixed potential that decreases cell voltage [11]. Pt, which is the catalyst for oxygen reduction, is the most active metal for dissociative adsorption of methanol and, at low temperature, it is poisoned by the CO produced by direct methanol oxidation. Both new membranes that are less permeable to methanol and CO-tolerant cathode catalysts are under investigation to solve, or at least reduce, the negative effects of methanol crossover [12–14].

Focusing on electrocatalyst to improve the catalytic activity of carbon supported PtRu, we prepared and characterized cryogel mesoporous carbons of different pore size distribution and report the results of their synthesis and characterization and the catalytic activity of supported PtRu on two mesoporous carbons of pore size >15 nm in passive and in active, i.e. forced-flow, DMFCs. Given that the *V–I* and *P–I* characteristics are strongly affected by the DMFC assembly (hot-pressing conditions, current collector materials and structures) and operating conditions (electrode loadings, methanol concentration and temperature), we also compared the catalytic activities of mesoporous carbon/PtRu systems to that of commercial Vulcan carbon/PtRu tested under the same conditions in active DMFCs (a-DMFCs) at different temperatures. The performance of the C656/PtRu anode in passive DMFCs (p-DMFCs) over long operating time, which is tailored to the volume and concentration of the CH_3OH reservoir, is also reported.

* Corresponding author. Tel.: +39 0512099798; fax: +39 0512099365.
E-mail address: marina.mastragostino@unibo.it (M. Mastragostino).

0378-7753/$ – see front matter © 2008 Elsevier B.V. All rights reserved.
doi:10.1016/j.jpowsour.2008.09.022

2. Experimental

The cryogel carbons were prepared by polycondensation of resorcinol (*R*) and formaldehyde (*F*) in ultrapure water (*W*) with Na_2CO_3 (*C*) as gelation catalyst, followed by water/*t*-butanol solvent exchange, freeze drying, pyrolysis and ball milling as reported in ref. [15], with molar ratios $R/F = 0.5$, $W/(R+F+C) = 5.7$ and $R/C = 500$. A unique solution batch was divided into five samples and the initial pH was adjusted to 6.19, 6.30, 6.43, 6.56 and 6.80; the resulting mesoporous carbons were labelled C619, C630, C643, C656 and C680, respectively.

PtRu (1:1) was chemically deposited on C656 and C619 ball-milled carbons as in ref. [15] and the Pt contents were experimentally determined after mineralization of the powders by the tin (II) chloride colorimetric method [16]. Nitrogen adsorption porosimetry measurements on bare carbons and on carbon/PtRu were carried out at 77 K with an Micromeritics ASAP 2020 system: the carbon powders were dried for 2 h at 120 °C before testing. The N_2 adsorption isotherms were analyzed by BET and DFT theories with a model of cylindrical pores.

XRD measurements were performed with a Philips PW1710 diffractometer, a Cu Kα (λ = 1.5406 Å) radiation source and Ni filter. The crystallite size (D_{220}) was evaluated by Scherrer's equation from the width of the 220 reflex. Scanning electron microscopy observations (SEM) and energy dispersion spectroscopy (EDS) were carried out with a Zeiss EVO 50 equipped with an energy dispersive X-ray analyser from Oxford INCA Energy 350 system. The Pt and Ru atomic % were evaluated by EDS.

The anodes were prepared by spraying 2-propanol-based inks containing home-made carbon/PtRu or commercial Vulcan XC72R (hereinafter called Vulcan)/PtRu (Electrochem Inc., 20%Pt, Pt:Ru = 1:1 as declared by supplier) onto two types of gas diffusion layers (GDLs): GEFC®-GDL3 carbon paper (CP) and ELAT®-GDL microporous layer on woven web (WW). The Pt content of the anodes ranged from 1.0 to 2.5 mg cm^{-2}. The cathodes were commercial ELAT V2.1 standard, single-side, gas diffusion electrode (GDE) with Pt black loading of 5.0 mg cm^{-2}. GDLs and GDE were from Hydro2Power.

Passive DMFCs fuelled with 1 M CH_3OH solution were built with the home-made mesoporous carbon/PtRu on CP and WW anodes and with the commercial GDE cathodes hot-pressed onto a Nafion® 117 (Hydro2Power) that had been treated as described in ref. [17]. When the CP were used, a small amount of 1 wt.% Nafion® aqueous solution was sprayed on top of the anodes (0.25 mg cm^{-2} dry Nafion®) just before hot-pressing onto the Nafion® membrane for better adhesion. The use of WW, which enables a more effective hot-pressing, did not require the addition of Nafion® on the top of the electrodes. The cells were held together by two acrylic plates with fixed stainless-steel current collectors; the 1 M CH_3OH solution was placed in a reservoir (1.5–1.9 mL) in the anode plate and the air diffused into the cathode through the openings of the cathode plate to air. Before testing the p-DMFCs (3 cm^2 area) at room temperature (RT), the p-DMFCs underwent activation by 1000 galvanostatic steps between open circuit condition (120 s) and high constant current (60 s), refreshing the CH_3OH solution in the reservoir every 100–150 steps. Chronoamperometry tests at different cell potentials (300 s at each potential followed by 300 s in open circuit voltage (OCV)) were performed to build the polarization curves and the current–power plots. Chronopotentiometry tests at different currents and chronoamperometry tests at different cell potential and at OCV were also performed for several hours to highlight the methanol crossover in the p-DMFC.

Membrane electrode assemblies (MEAs) for a-DMFCs (5 cm^2 area) were installed in an Electrochem fuel cell test-fixture connected to an Electrochem MTS-A-150/EC-DM test-station. MEAs for a-DMFC were assembled with the carbon/PtRu sprayed only onto WW substrate as anode and with the commercial GDE as cathode. A 1 M CH_3OH solution, at the same temperature as the cell's and at atmospheric pressure, fed the anode compartment and dry O_2 at 1 bar and RT fed the cathode. CH_3OH and O_2 flow rates were 5 and 250 mL min^{-1} and the tests were performed at 30, 60 and 80 °C. Before testing, the a-DMFCs underwent activation at high current at 60 °C for 4 h and, after temperature changes, the conditioning time under reactant fluxes was 30 min. Chronoamperometry tests at different cell potentials (300 s at each potential followed by 300 s in OCV) were carried out to build the *V–I* and *P–I* characteristics at different temperatures.

The specific current and power of all DMFCs were calculated by considering only the weight of Pt in PtRu at the anode. For the specific values of the a-DMFCs with Vulcan/PtRu anodes, we used the Pt content (30 wt.%) resulting from our tin (II) chloride colorimetric analysis, supported by XRD and EDS investigations, which also revealed a higher Pt/Ru ratio than that declared.

Active DMFCs were also characterized by electrochemical impedance spectroscopy (EIS). The impedance spectra were usually between 100 kHz and 10 mHz, with 10-step/decade in OCV and under different DC potentials superimposed on the 10 mV sinusoidal wave. The DMFC tests were performed with multichannel Bio-Logic VSP and VMP potentiostat/galvanostats, the latter equipped with 2 A and 20 A boosters. For EIS measurements a Bio-Logic VSP potentiostat and a PAR 270A potentiostat combined with a Solartron 1255 frequency response analyzer were used.

The CO-stripping tests were performed with a Radiometer PGZ301 Voltalab potentiostat/galvanostat in H_2SO_4 0.1 M at RT by flowing CO for 10 min without electrode polarization, followed by 10 min at 0.24 V vs NHE always in CO bubbling. The CO flow was then switched off and the electrode was kept at the same potential by flowing Ar for 20 min after that the potential was scanned at 50 mV s^{-1} from 0.24 V to 1.2 V vs NHE. The electrocatalytic layer on the glassy carbon working electrode (3 mm diameter) was obtained by evaporation of 5 μL of aqueous inks containing carbon/PtRu (0.7 mg_{Pt} mL) and Nafion (carbon:Nafion = 4:1); the Pt loading on the electrode was 3.5 μg. The reference electrode was $Hg/HgSO_4/K_2SO_4$ (saturated solution) and the counterelectrode was a Pt wire.

3. Results and discussion

The chemistry involved in sol–gel synthesis of carbons by resorcinol-formaldehyde is strongly influenced by pH [18,19]. We had already investigated xero- and cryogel carbons synthesized in different *D* and *R*/*C* conditions by maintaining the initial pH value in the different samples constant [15]. The best results were with the sample having $R/F = 0.5$, $D = 5.7$ and $R/C = 500$. Starting from these ratios, we changed the pH of the initial solution before gelation. The porosimetric analysis of the cryogel carbons gave the results shown in Fig. 1 and Table 1, where the data of Vulcan carbon are also reported for comparison. Fig. 1 shows the incremental volume vs pore size of the different carbons by DFT pore size analysis in the meso-macro pore regions. This analysis shows the contribution to the volume of pores of different sizes, which change with the initial pH according to ref. [19]. Porosimetric analysis on C656/PtRu and C619/PtRu (not reported here) demonstrated that catalyst deposition does not modify pore size distribution and only slightly decreases the pore volume of the carbon without affecting the area determined by pores in the 2–100 nm range. Table 1 shows the total pore volume of the carbons (V_{tot}), evaluated from the volume of gas adsorbed at $p/p^\circ = 0.99$ relative pressure, the total

Table 1
Total pore volume, total specific BET area, specific pore volume and surface area in the 2–100 nm range and in the 2–50 nm range from DFT analysis and the mostly central pore size range of cryogel and commercial Vulcan carbon powders.

Carbon	V_{tot} ($cm^3\,g^{-1}$)	S_{BET} ($m^2\,g^{-1}$)	$V_{2-100\,nm}$ ($cm^3\,g^{-1}$)	$V_{2-50\,nm}$ ($cm^3\,g^{-1}$)	$A_{2-100\,nm}$ ($m^2\,g^{-1}$)	$A_{2-50\,nm}$ ($m^2\,g^{-1}$)	d (nm)
C680	0.50	362	0.24	0.23	114	114	10
C656	1.14	565	0.72	0.68	168	166	20
C643	1.15	504	0.80	0.74	146	142	15–35
C630	1.15	515	0.80	0.68	124	116	20–45
C619	1.22	527	0.86	0.60	114	100	35–65
Vulcan	0.51	221	0.23	0.12	26	22	5–90

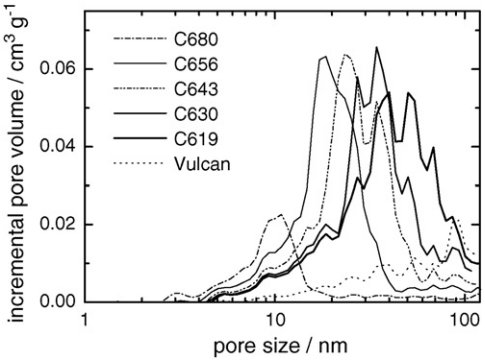

Fig. 1. Incremental volume vs pore size of mesoporous cryogel carbons synthesized at different pH values (6.80, 6.56, 6.43, 6.30 and 6.19) and of Vulcan carbon.

specific area from BET analysis (S_{BET}) and the specific pore volume and surface area from DFT analysis in the pore diameter range of 2–100 nm and in the mesopore range (2–50 nm); a rough evaluation of the range in which pore dimension is mostly centred (d) is also reported. The V_{tot} and S_{BET} values also comprise the micropore contribution. The carbon synthesized at pH 6.80 presents low pore volume and surface area because the condensation reaction, which forms cross-links, is hindered at high pH values and the resulting structure may collapse during drying and pyrolysis. By contrast, the strong porous structure formed by the H^+-catalyzed condensation at pH 6.19 remains even after pyrolysis. Among the synthesized carbons we selected C656, with the highest area and pore size centred at 20 nm, and C619, with a slightly lower area and a porosity more distributed in the range 35–65 nm, for PtRu deposition. These substrates should favour catalyst dispersion and three-phase contact among PtRu, Nafion ionomers and reactants; they have a surface area higher than that of Vulcan and, more importantly, a higher fraction of this area is in the mesoporous region, as the data in Table 1 display.

The SEM images of C656/PtRu and C619/PtRu are quite similar, evincing small particles and aggregates. Fig. 2a shows, for example, the SEM image of C656/PtRu. The Pt contents and percentages over the total sample weight, evaluated on mineralized samples, was 31% and 28% for two samples of C656/PtRu and 23% for C619/PtRu. EDS analysis confirmed the Pt:Ru atomic ratio near 1:1 for all samples. The values of the cell parameter (a_{220}) from the XRD patterns shown in Fig. 2b are consistent with EDS results and are all reported in Table 2, where the crystallite size (D_{220}) is also reported. The cell

Table 2
Crystallite size (D_{220}), fcc cell parameter (a_{220}) from XRD patterns and Pt-to-Ru molar ratio of C656/PtRu and C619/PtRu powders.

Catalyst	D_{220} (nm)	a_{220} (Å)	Pt:Ru (at %)
C656/PtRu (Pt = 28 wt.%)	2.8	3.877	55:45
C619/PtRu (Pt = 23 wt.%)	2.7	3.893	58:42

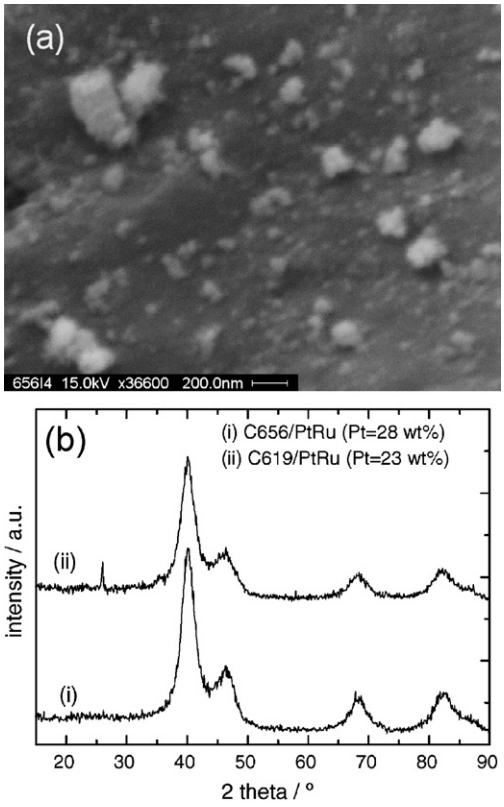

Fig. 2. (a) SEM image of C656/PtRu powder; (b) XRD patterns of C656/PtRu and C619/PtRu powders.

parameter of C656/PtRu shows that more Ru is alloyed with Pt in the fcc cell than in C619/PtRu.

Fig. 3 shows, as an example, the polarization curves and the P–I plots of the passive C656/PtRu/Nafion 117/Pt black (p-DMFC48). These data were collected after the activation of the DMFC (see Section 2), when stabilization of performance was achieved. The specific maximum power (P_{max}) for p-DMFC48 was 2.8 W g^{-1} and the corresponding current, I_{max}, was 11.2 A g^{-1}. Fig. 4 displays the V–I and P–I plots of p-DMFCs with C619/PtRu sprayed on CP and on WW, and Table 3 shows the performance of the passive DMFCs assembled with different anodes catalysts on different substrates (CP or WW) after 1000 activation steps. The Table displays the I and P values at the cell potential of 0.45 V, i.e. in the region of activation polarization, and at the potential corresponding to the P_{max}, called V_{max}, in the region of ohmic polarization. WW, instead of CP, enable MEA assembly under higher pressure, with a consequent decrease in ohmic losses but also the unwanted decrease of the reaction rate [20], particularly in the case of C619/PtRu on WW which, however, shows the best results in terms of specific maximum power. The notable CO_2 evolution from the anode and the water production at the cathode hinder the transport of methanol

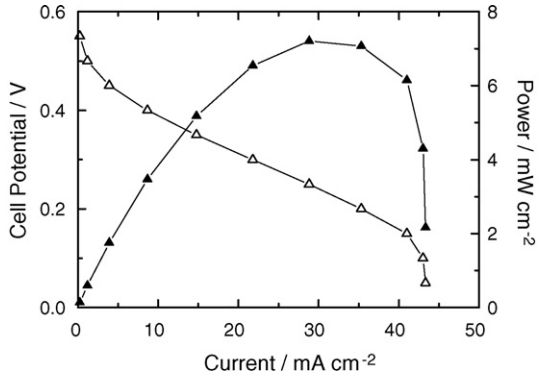

Fig. 3. *V–I* and *P–I* plots of the passive C656/PtRu (Pt = 31 wt.%, 2.54 mg cm^{-2})/Nafion 117/Pt black (p-DMFC48) with C656/PtRu on CP.

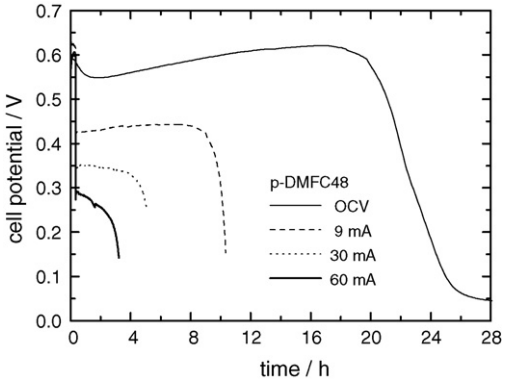

Fig. 5. Potential profiles over time at OCV and under discharge at different constant current of the C656/PtRu (Pt = 31 wt.%, 2.54 mg cm^{-2})/Nafion 117/Pt black (p-DMFC48) with 1.9 mL of 1 M CH_3OH in the reservoir.

and oxygen that, at the highest currents, become so critical that the cell potential sharply decreases and it is impossible to complete the *P–I* plots.

Fig. 5 shows the cell potential profiles over time at OCV and under discharge at different constant currents of p-DMFC48. These voltage profiles show that p-DMFC, which has a CH_3OH reservoir that in the absence of crossover and evaporation should provide sufficient fuel to allow about 1000 coulombs to flow, is unable to provide power after 20–25 h. Under constant current of 9, 30 and 60 mA the fuel is exhausted after 10, 5 and 3 h, even if it should in theory be consumed after 31, 9 and 4.5 h. The increase in the ratio between the practical and the theoretical utilization time at increasing current indicates that methanol crossover exerts more effect on cell performance at low currents.

We estimated the faradic and the energy efficiencies of these DMFCs as $\eta = Q/6\,V\,C\,F$ and $\zeta = V\,\eta/1.18$, respectively [21], where Q is the discharge capacity, V the volume of CH_3OH solution, C the CH_3OH concentration, F the Faraday constant and V the discharge voltage of the DMFC. At 9, 30 and 60 mA the faradic efficiency percentage was 28%, 46% and 54%, thus higher at higher current. The energy efficiency percentage was near 10%, a low value due to the intrinsic low potential of the cell resulting from methanol crossover. Data from measurements over time at constant cell potentials gave the same results, which compare well with some reported in literature [21,22].

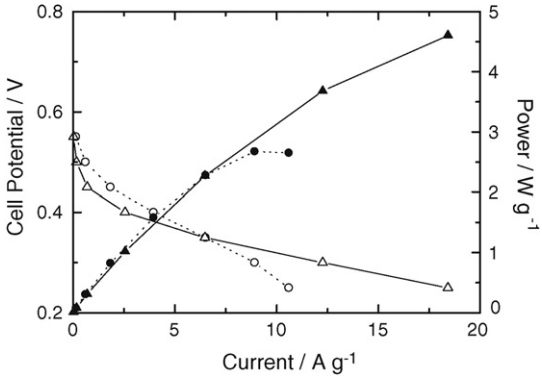

Fig. 4. *V–I* and *P–I* plots of the passive C619/PtRu (Pt = 23 wt.%, 1.45 mg cm^{-2})/Nafion 117/Pt black (p-DMFC54 and p-DMFC56) with CP (circles) and WW (triangles) as anode gas diffusion layers, respectively.

As noted above, p-DMFC assembly and the fact that the cell can be tested only at RT limit the performance of the electrocatalysts we developed, especially at high currents. We thus tested the anodes in active DMFCs in order to evaluate their catalytic activity at higher temperatures than RT. Fig. 6a shows the *V–I* and *P–I* characteristics of the C656/PtRu/Nafion 117/Pt black a-DMFCs at 30, 60 and 80 °C; the results for power and current density at different potentials are shown in Table 4. These results were compared to those of a-DMFC assembled with commercial Vulcan/PtRu, whose *V–I* and *P–I* plots are in Fig. 6b. It is evident from the Fig. 6 and Table 4 that the C656/PtRu catalytic system performs better than Vulcan/PtRu. At 80 °C the required amount of Pt per kW estimated at 0.4 V cell voltage was 31 g kW^{-1} for the C656/PtRu, a value less than half of that of Vulcan/PtRu (77 g kW^{-1}). It is worth noting that the specific current and power for the latter were calculated on the basis of the Pt% resulting from our analysis described in Section 2 and which differed from that declared by the supplier. In any case, even given the nominal Pt percentage, the C656/PtRu catalytic system is still better. The data at different temperatures were used to estimate the activation energy of the electron-transfer process (evaluated using the current recorded at 0.5 V) of 26 and 33 kJ mol^{-1}, respectively for the a-DMFC with C656/PtRu and Vulcan/PtRu as anode: the easier electron transfer at the C656/PtRu electrocatalyst confirms the above results.

Further confirmation was given by the results from EIS reported in Fig. 7. Fig. 7a shows the spectra of the C656/PtRu/Nafion 117/Pt black a-DMFC at 0.25 V at different temperatures and Fig. 7b the

Table 3
I and *P* values at the cell potential of 0.45 V, I_{max} and P_{max} of different p-DMFCs.

p-DMFC	Anode property			*I* and *P* at 0.45 V				I_{max} and P_{max}				
	Substrate	Catalyst	(mg_{Pt} cm^{-2})	(mA cm^{-2})	(A g^{-1})	(mW cm^{-2})	(W g^{-1})	V_{max}	(mA cm^{-2})	(A g^{-1})	(mW cm^{-2})	(W g^{-1})
52	CP	C656/PtRu	1.50	1.8	1.2	0.8	0.5	0.25	19.9	13.2	5.0	3.3
61	WW	C656/PtRu	1.76	3.9	2.2	1.8	1.0	0.25	29.8	16.9	7.4	4.2
54	CP	C619/PtRu	1.45	2.7	1.8	1.2	0.8	0.30	12.9	8.9	3.9	2.7
56	WW	C619/PtRu	1.41	1.0	0.7	0.5	0.3	0.25	26.0	18.4	6.5	4.6

Table 4
P and I at 0.4 V, P_{max} and I_{max} of the a-DMFCs with C656/PtRu (Pt = 28 wt.%) and Vulcan/PtRu (Pt = 30 wt.%) as anode at different temperatures.

Cell voltage			C656/PtRu (Pt = 28 wt.%, 1.27 mg cm^{-2})			Vulcan/PtRu (Pt = 30 wt.%, 1.08 mg cm^{-2})		
			30 °C	60 °C	80 °C	30 °C	60 °C	80 °C
0.4 V	P	mW cm^{-2}	13	29	40	3	6	14
		W g^{-1}	10	23	32	3	6	13
	I	mA cm^{-2}	33	72	101	7	15	34
		A g^{-1}	26	57	80	6	14	31
V_{max}	P_{max}	mW cm^{-2}	17	35	47	5	9	17
		W g^{-1}	14	28	37	4	9	16
	I_{max}	mA cm^{-2}	69	118	157	19	42	69
		A g^{-1}	54	93	124	18	39	64

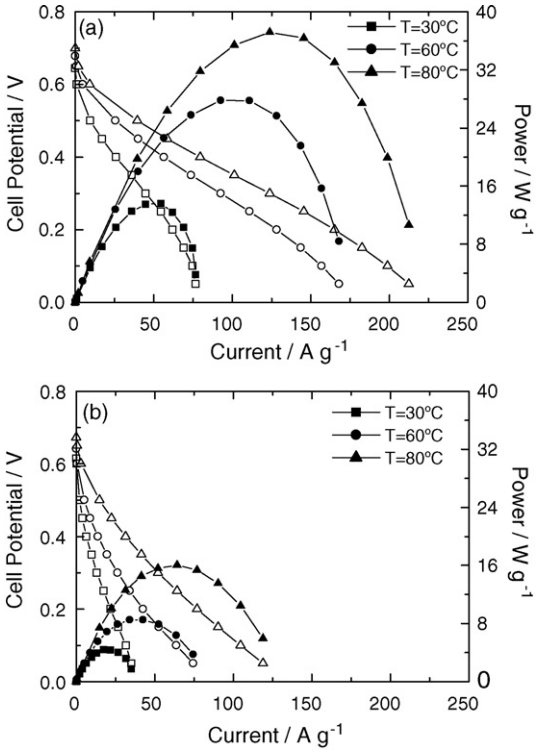

Fig. 6. V–I and P–I characteristics at 30, 60 and 80 °C of a-DMFCs fed with 1 M CH_3OH (ambient pressure) and dry O_2 (1 bar) at 5 and 250 mL min^{-1} flow rates, respectively: (a) C656/PtRu (Pt = 28 wt.%, 1.27 mg cm^{-2})/Nafion 117/Pt black; (b) Vulcan/PtRu (Pt = 30 wt.%, 1.08 mg cm^{-2})/Nafion 117/Pt black.

spectra of the two a-DMFCs with C656/PtRu and Vulcan/PtRu as anodes at 60 °C and 0.25 V. The spectra show a shift from the origin due to ohmic resistance, a small 45° region representing the electrolyte impedance in the catalytic layer and a typical RC response due to the electrochemical reactions. The inductive behaviour, which is related to the relaxation/adsorption of CO, is distinct only for the DMFC with the Vulcan/PtRu anode. Fig. 7a shows that the resistance associated with the reaction kinetics decreases with increasing temperature (from 2.8 to 0.8 Ω cm^2), as expected; the 45° response is restricted to lower impedance, suggesting a lower electrolyte resistance in the catalyst layer [23]. Ohmic resistance (1.15 Ω cm^2) remains constant with temperature, indicating that other important contributing factors to resistance have to be considered. The comparison of the two spectra in Fig. 7b, which were recorded at the same temperature and potential, shows the higher resistance (roughly thrice) of the electrode processes occurring at the Vulcan/PtRu anode, and the wide inductive process at low frequency indicates a more difficult CO removal than in C656/PtRu [24,25]. These factors may explain the low performance of the commercial catalytic system with respect to C656/PtRu.

To further support the data indicating that C656/PtRu is a better catalyst system than Vulcan/PtRu, we evaluated the specific electrochemical active surface area (ECA) of the two systems by CO-stripping voltammetry, according to the equation ECA = $Q_{CO}/(Q\, m_{Pt})$, where Q_{CO} is the measured charge for CO oxidation, Q is the charge for the oxidation of CO adsorbed on 1 cm^2 of Pt and m_{Pt} the Pt loading in the electrode. Given that the CO electrooxidation process at carbon/PtRu electrocatalysts still lacks a detailed picture [26,27], we prefer to give only a relative value of C656/PtRu ECA: it was about twice that of Vulcan/PtRu as per the performance of the two DMFCs.

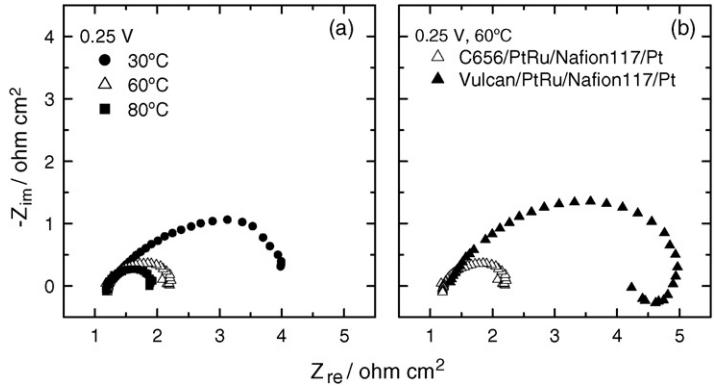

Fig. 7. Impedance spectra of DMFCs fed with 1 M CH_3OH (ambient pressure) and dry O_2 (1 bar) at flow rates of 5 and 250 mL min^{-1} from 1 kHz to 100 mHz. (a) C656/PtRu (Pt = 1.27 mg cm^{-2})/Nafion 117/Pt black at 0.25 V at different T and (b) C656/PtRu (Pt = 1.27 mg cm^{-2})/Nafion 117/Pt black and Vulcan/PtRu (Pt = 1.08 mg cm^{-2})/Nafion 117/Pt black at 60 °C and 0.25 V.

4. Conclusions

All characterization results of the developed catalytic systems clearly demonstrated that the in-house synthesized mesoporous carbons are more effective than Vulcan carbon as supports for PtRu. While Vulcan/PtRu in a-DMFCs at 80 °C provided P_{max} and I_{max} values of 16 W g^{-1} and 64 A g^{-1}, C656/PtRu in the same conditions delivered a maximum specific power of 37 W g^{-1} and a related current of 124 A g^{-1}. In terms of mass of Pt per kW, the required amount of Pt for C656/PtRu, estimated at 0.4 V cell voltage and 80 °C was 31 g kW^{-1}, a value less than half of that of Vulcan carbon/PtRu (77 g kW^{-1}).

Acknowledgements

Research funded by MIUR under the Italian Project FISR "Development of composite protonic membranes and of new electrode configurations for fuel cells with polymer electrolyte".

References

[1] http://www.fuelcelltoday.com.
[2] http://www.dtienergy.com.
[3] H.A. Gasteiger, J. Garche, in: G. Ertl, et al. (Eds.), Handbook of Heterogeneous Catalysis, 2nd ed., Wiley, 2008.
[4] H. Liu, C. Song, L. Zhang, J. Zhang, H. Wang, D.P. Wilkinson, J. Power Sources 155 (2006) 95–110.
[5] G.-G. Park, T.-H. Yang, Y.-G. Yoon, W.-Y. Lee, C.-S. Kim, Int. J. Hydrogen Energy 28 (2003) 645–650.
[6] Y. Takasu, T. Kawaguchi, W. Sugimoto, Y. Murakami, Electrochim. Acta 48 (2003) 3861–3868.
[7] K. Nam, D. Jung, S.-K. Kim, D. Peck, S. Ryu, J. Power Sources 173 (2007) 149–155.
[8] N. Jha, A. Leela Mohana Reddy, m.M. Shaijumon, N. Rajalakshmi, S. Ramaprabhu, Int. J. Hydrogen Energy 33 (2008) 427–433.
[9] E. Yoo, T. Okada, T. Kizuka, J. Nakamura, J. Power Sources 180 (2008) 221–226.
[10] M.P. Hogarth, T.R. Ralph, Platinum Met. Rev. 46 (2002) 146–164.
[11] S. Eccarius, B. Lee Garcia, C. Hebling, J.W. Weidner, J. Power Sources 179 (2008) 723–733.
[12] V. Neburchilov, J. Martin, H. Wang, J. Zhang, J. Power Sources 169 (2007) 221–238.
[13] E. Antolini, T. Lopes, E.R. Gonzales, J. Alloy Compd. 461 (2008) 253–262.
[14] C.W.B. Bezerra, L. Zhang, K. Lee, H. Liu, A.L.B. Marques, E.P. Marques, H. Wang, J. Zhang, Electrochim. Acta 53 (2008) 4937–4951.
[15] C. Arbizzani, S. Beninati, E. Manferrari, F. Soavi, M. Mastragostino, J. Power Sources 172 (2007) 578–586.
[16] G.H. Ayres, A.S. Meyer Jr., Anal. Chem. 23 (1951) 299–334.
[17] C. Arbizzani, M. Biso, E. Manferrari, M. Mastragostino, J. Power Sources 178 (2007) 584–590.
[18] S.A. Al-Muhtaseb, J.A. Ritter, Adv. Mater. 15 (2003) 101–114.
[19] C. Lin, J.A. Ritter, Carbon 35 (1997) 1271–1278.
[20] Z.X. Liang, T.S. Zhao, C. Xu, J.B. Xu, Electrochim. Acta 53 (2007) 894–902.
[21] J.G. Liu, T.S. Zhao, R. Chen, C.W. Wong, Electrochem. Commun. 7 (2005) 288–294.
[22] D. Chu, R. Jiang, Electrochim. Acta 51 (2006) 5829–5835.
[23] J.T. Müller, P.M. Urban, W.F. Hölderich, J. Power Sources 84 (1999) 157–160.
[24] A. Oedegaard, J. Power Sources 157 (2006) 244–252.
[25] R. Makharia, M.F. Mathias, D.R. Baker, J. Electrochem. Soc. 152 (2005) A970–A977.
[26] T. Vidaković, M. Christov, K. Sundmacher, Electrochim. Acta 52 (2007) 5606–5613.
[27] F. Maillard, A. Bonnefont, M. Chatenet, L. Guétaz, B. Doisneau-Cottignies, H. Roussel, U. Stimming, Electrochim. Acta 53 (2007) 811–822.